Molecular structural property and potential energy dependence on nonequilibrium-thermodynamic state point of liquid n-hexadecane under shear

Huan-Chang Tseng, Rong-Yeu Chang, and Jiann-Shing Wu

Citation: The Journal of Chemical Physics **134**, 044511 (2011); doi: 10.1063/1.3541825
View online: http://dx.doi.org/10.1063/1.3541825
View Table of Contents: http://scitation.aip.org/content/aip/journal/jcp/134/4?ver=pdfcov
Published by the AIP Publishing

Molecular structural property and potential energy dependence on nonequilibrium-thermodynamic state point of liquid *n*-hexadecane under shear

Huan-Chang Tseng,[1,a)] Rong-Yeu Chang,[2] and Jiann-Shing Wu[3]
[1]*Molecular Dynamics Technology Co. Ltd., Hsinchu County 30265, Taiwan*
[2]*Department of Chemical Engineering, National Tsing Hua University, Hsinchu 30043, Taiwan*
[3]*Department of Applied Chemistry, National Chiao Tung University, Hsinchu 30010, Taiwan*

(Received 21 July 2010; accepted 22 December 2010; published online 24 January 2011)

Extensive computer experiments have been conducted in order to shed light on the macroscopic shear flow behavior of liquid *n*-hexadecane fluid under isobaric–isothermal conditions through the nonequilibrium molecular dynamic methodology. With respect to shear rates, the accompanying variations in structural properties of the fluid span the microscopic range of understanding from the intrinsic to extrinsic characteristics. As drawn from the average value of bond length and bond angle, the distribution of dihedral angle, and the radius distribution function of intramolecular and intermolecular van der Waals distances, these intrinsic structures change with hardness, except in the situation of extreme shear rates. The shear-induced variation of thermodynamic state curve along with the shear rate studied is shown to consist of both the quasiequilibrium state plateau and the nonequilibrium-thermodynamic state slope. Significantly, the occurrence of nonequilibrium-thermodynamic state behavior is attributed to variations in *molecular potential energies*, which include bond stretching, bond bending, bond torsion, and intra- and intermolecular van der Waals interactions. To unfold the physical representation of extrinsic structural deformation, under the aggressive influence of a shear flow field, the molecular dimension and appearance can be directly described via the squared radius of gyration and the sphericity angle, $R_g{}^2$ and φ, respectively. In addition, a specific orientational order S_x defines the alignment of the molecules with the flow direction of the *x*-axis. As a result, at low shear rates, the overall molecules are slightly stretched and shaped in a manner that is increasingly ellipsoidal. Simultaneously, there is an obvious enhancement in the order. In contrast to high shear rates, the molecules spontaneously shrink themselves with a decreased value of $R_g{}^2$, while their shape and order barely vary with an infinite value of φ and S_x. It is important to note that under different temperatures and pressures, these three parameters are integrated within a molecular description in response to thermodynamic state variable of density and rheological material function of shear viscosity. © *2011 American Institute of Physics*. [doi:10.1063/1.3541825]

I. INTRODUCTION

The molecular nature of soft matter and liquid fluids, with respect to transportation, deformation, and orientation, crucially appears as a mere academic curiosity. Nonequilibrium molecular dynamic (NEMD) simulations are exclusively suited to study the relation of macroscopically observable flow behavior to the accompanying changes in microscopic structures. Differing with other computational technologies, the NEMD simulation provides a reliable valuable description and information at a molecular level, regarding how molecules stretch, shrink, align, and rotate in response to the thermodynamic and rheological phenomena.

The NEMD simulation's algorithm was originally developed by combining the SLLOD equations of motion (named after the Kewpie Doll by Hoover due to the matrix transposition of the Dolls' tensor which is dyadic product of atomic position and momenta) with the sliding brick periodic boundary condition (proposed by Lees and Edwards).[1–3] Such simulations have been conducted for the purpose of investigating the steady shear flow of various fluids from simple to increasingly complex, including argon,[4,5] *n*-alkane,[6–20] alcohol,[21] ketone,[22] and water.[23] Notably, other more complicated fluids, such as polymer melts,[24–31] blended polymeric mixtures,[32,33] and molten alkali halides,[34,35] can also be carried out. Surprisingly, on the nanoscale, these manifold fluids are capable of exhibiting highly interesting behaviors, for example, shear thinning and nonequilibrium-thermodynamic state (NTS) behaviors.[7,16,36] The application of NEMD simulations has traditionally focused on steady state shear flows to predict their thermodynamic rheological, and structural properties.[25,37]

Most NEMD investigations have concentrated on the fundamental steady state shear flow field. As a rule, the primary variables for induced variations of thermodynamic, rheological, and structural properties are shear rate, temperature, pressure, and molecular structure/constitution. Those discussions have stressed the thermodynamic state variable,

a)Author to whom correspondence should be addressed. Present address: Tai Yuen Hi-Tech Industrial Park 8F-2, No.32, Taiyuan St., Chupei City, Hsinchu County, 30265, Taiwan. Electronic mail: ivortseng@moldex3d.com. Tel.: +886-3-560-0199 ext 502. Fax: +886-3-560-0198.

including density and pressure, as well as the rheological material function, including shear viscosity and normal stress coefficient. In addition, the structural properties studied with regard to conformations and configurations involve molecular dimension (e.g., end-to-end distance and radius of gyration), orientation tensors, and inertia tensors. Furthermore, applying computer visualization technology, NEMD researchers have clearly produced a realistic molecular deformation history in the context of shear and elongation flows.[30] Accordingly, exploration in molecular motion is vital with regard to the industrial perspective, namely, Bio-MEMS, nanolubrication, and nanotribology.

The NEMD system under *isothermal* conditions involves two thermodynamic systems, constant-volume nonequilibrium molecular dynamic (*NVT*-NEMD) and constant-pressure nonequilibrium molecular dynamic (*NPT*-NEMD).[2,7,38] Concerns surrounding of nonequilibrium-thermodynamic state behavior have been generally limited to constant-volume NEMD systems: the variation in pressure, with respect to the shear rate, is relevant to intermolecular and intramolecular potential energies. These *NVT*-NEMD studies may not be convenient for related practical applications when there are complementing experimental observations at known temperature and pressure.[6,32,39] Regrettably, only a few attempts have been made to probe *NPT*-NEMD simulations[7,32,38,40] because of numerical instability: the instantaneous pressure drifts suddenly to generate large instantaneous volume fluctuations.[41]

To resolve this numerical instability, Wang and Fichthorn[41] proposed a modified pressure method to obtain an effectively stable numerical solution as regards the volume. Nevertheless, in *NPT*-NEMD systems, the shear-induced density variation dependence on those molecular potential energies has *not* been consistently analyzed. In reviewing the NEMD literature, the effects of temperature and pressure on thermodynamic states and rheological properties have been discussed and have provided great insights.[9,16,42] However, the structural properties under the influence of temperature and pressure have *not* been investigated so far. Substantially, these arguments are our main research motivation.

More recently, we reported a series of NEMD studies[16–18] detailing the nonequilibrium-thermodynamic states and rheological behaviors of liquid *n*-hexadecane under steady state shear flow, including nonequilibrium-thermodynamic state behavior, shear thinning phenomenon, and normal stress effects. In addition, the shear viscosity against shear-rate flow curves and the nonequilibrium-thermodynamic state curves can be spectacularly normalized as: *temperature-, pressure-*, and *density-invariant master curves*.

Drawing on our previous constant-pressure NEMD simulations,[16–18] an objective is to propose a plausible microscopic understanding of the observed macroscopic shear flow phenomena. This study was motivated by the need to present a complete discussion on changes in structural properties with respect to shear rate, temperature, and pressure. That being said, the aim of this article is twofold. The first focus was to clearly present the shear-induced variation in molecular conformations (bond length, bond angle, dihedral angle distribution, and intra- and inter-radius distribution functions) with respect to molecular potentials (bond stretching, bond bending, torsion, and intra- and intermolecular distances of van der Waals interaction). More importantly, we further analyze, in a constant-pressure NEMD system, how different molecular potential energies contribute to a nonequilibrium-thermodynamic state such that the shear-induced change in density consists of the approached equilibrium state plateau and the nonequilibrium-thermodynamic state regime.

The second—and major—focus was to reveal the physical representation of a whole molecular chain undergoing structural deformation during shear flow, including molecular dimension, molecular appearance, molecular orientation described by the squared radius of gyration, the sphericity angle, and the orientational order. Therefore, we provide a molecular picture of dramatic variation of these properties, with respect to shear rate, as a function of temperature and pressure. This offers useful information for a better molecular understanding of macroscopic properties, i.e., thermodynamic state variable of density and rheological material function of shear viscosity.

The rest of the article is organized as follows. In Sec. II, we briefly describe simulation detail involving molecular potential models, simulation techniques, and structural properties. After that, we present results for the above loci in Sec. III. Finally, conclusions are given in Sec. IV.

II. SIMULATION DETAILS

Our previous article[16–18] provided details about the molecular model and simulation method. The constant-pressure (isobaric–isothermal or *NPT*) NEMD simulations[2,43] used a set of realistic Ryckaert–Bellemans molecular potentials[44] improved by Chynoweth and Michopoulos (CM).[8,45] The CM model can offer functions and parameters in order to describe the *van der Waals* and *covalent bonding* interactions, whereby molecular chains are coarse-grained with spherical interaction sites and regarded as *methylene* (CH_2) groups, namely, the *united atom*.

The van der Waals interaction can be represented by the 12–6 Lennard-Jones (LJ) potentials.[45] The covalent bonding interaction involves stretching, bending, and torsion motions. The stretching potential connects two CH_2 groups using harmonic spring potential with an *equilibrium bond length* of 0.153 nm.[8,46] The bending potential is described by the Taylor series' cubic term expansion of a bending angle deviation with an *equilibrium bond angle* of 109.47°.[8,46] The torsion potential is expressed by a fifth-order cosine polynomial of a dihedral angle.[44]

The NEMD algorithm was originally developed by combining the SLLOD equation of motion with the Lees–Edwards sliding brick periodic boundary condition.[3] A shear rate $\dot{\gamma}$ was imposed on the fluid to characterize the shear flow field, where $\dot{\gamma}$ was related to the streaming velocity v_x in the x-direction, namely, $\dot{\gamma} = \partial v_x/\partial y$. The equation of motion can be implemented using the Leapfrog–Verlet scheme proposed by Macgowan and Heyes.[47] For convergence while solving differential equations numerically, the magnitude of time step, dt, is *inversely* proportional to $\dot{\gamma}$ from 1.0 to 0.1 fs.[16,48] Each calculation was performed using an Intel Core I7

Processor with clock speed of 2.66 GHz. The needed central processing unit time per running million-timestep was about a half day.

The radial distribution function (RDF) (Refs. 18 and 28) is generally, abbreviated $g(r)$, as follows:

$$g(r) = \frac{\Sigma_{i=1}^{N}\Sigma_{j>i}^{N}\delta(|\mathbf{r} - \mathbf{r}_{ij}|)}{4\pi r^2 N\rho}, \tag{1}$$

where $\mathbf{r}$ is the orientation of the separation vector with its distance r, $\mathbf{r}_{ij}$ is the distance vector between the centers of the masses of molecules i and j, N is the total number of molecules, ρ is the density of the fluid, and δ is the delta symbol. This function implies the probability of finding two molecules at a separation distance r. At a *large* intermolecular distance, $g(r) = 1$. Frequently, the characteristics of $g(r)$ curves can be useful in distinguishing a pure material's phase states between gas, liquid, and solid.[49] In this present study, we examine the effect of shear rates on the resulting $g(r)$ curves, including both intramolecular and intermolecular van der Waals interactions. The intermolecular interaction occurs between CH_2 groups of different chains, and the intramolecular interactions between CH_2 groups in the same chain are separated by more than three CH_2 groups.

The squared radius of gyration R_g^2 is a useful measure of the average size of a flexible molecular chain.[50] It is conveniently expressed in terms of inertia tensor $I_{\alpha\beta}$:[51]

$$I_{\alpha\beta} = \sum_{j=1}^{n_b} m_j \left(R_j^2\delta_{\alpha\beta} - R_{j\alpha}R_{j\beta}\right), \tag{2}$$

$$R_g^2 = \frac{1}{2M}\left(I_{xx} + I_{yy} + I_{zz}\right), \tag{3}$$

where I_{xx}, I_{yy}, and I_{zz} are the x-, y-, and z-principal axes of inertia tensor, respectively. $M = \Sigma_{j=1}^{n_b} m_j$, where m_j is the mass of site j and n_b is the number of sites per chain molecule ($n_b = 16$ for an n-hexadecane molecule). The sum is over the entire site j of molecule i, R_j is the magnitude of the $\mathbf{R}_j$ vector of site j from the center-of-mass of molecule i, $\mathbf{r}_{\mathrm{cm},i}$, i.e., $\mathbf{R}_j = \mathbf{r}_j - \mathbf{r}_{\mathrm{cm},i}$, $\mathbf{r}_j$ is the position of site j from the origin, $R_{j\alpha}$ and $R_{j\beta}$ are components of $\mathbf{R}_j$, the subscript is coordinates, $\alpha, \beta = x, y, z$, and $\delta_{\alpha\beta}$ is the Kronecker delta.

At equilibrium, the shape of the molecular orientation distribution is thought to be a perfect sphere of a random coil. When the shear deformation is exerted upon molecules, the shape becomes increasingly ellipsoidal. In this study, the flow direction is from the x-axis and the x-principal axis of the coil should be the smallest moment of inertia.

For simplicity, the ellipsoidal nature of molecule i can be quantified by the sphericity angle φ, which depends on the principal axes of the inertia tensor above,[6]

$$\varphi = \tan^{-1}\left(\frac{I_{xx}}{0.5(I_{yy} + I_{zz})}\right). \tag{4}$$

Note that the perfect sphere's three principal axes with the same moments, $I_{xx} = I_{yy} = I_{zz}$, correspond to a value of $\varphi = 45^{\circ}$; this value also characterizes the Newtonian behavior. $\varphi < 45^{\circ}$ means that the molecular orientation distribution is an ellipsoidal shape.

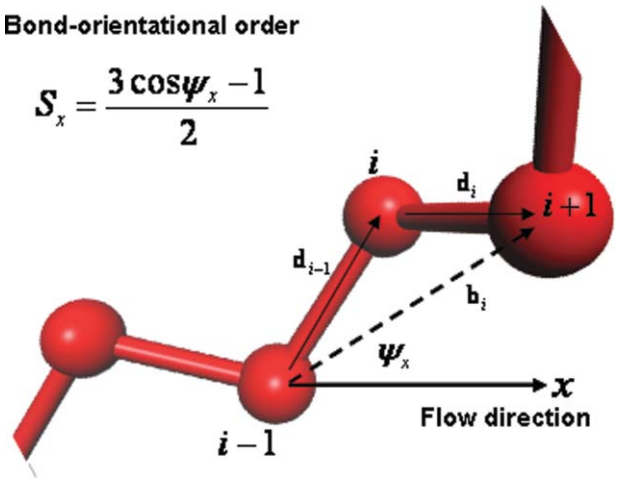

FIG. 1. A schematic representation of bond-orientational order S_x of a chain along the flow direction of x-axis.

In order to investigate the degree of orientation for the individual molecular chain along the shear flow direction (x-axis), the orientational order parameter S_x is defined by the second order Legendre polynomial[52,53]

$$S_x = \frac{3\cos^2\psi_x - 1}{2}, \tag{5}$$

where ψ_x is the angle between sub-bond vector $\mathbf{b}_i$ and the x-axis.

As shown in Fig. 1, $\mathbf{b}_i$ is formed by connecting the centers of two adjacent bonds $i - 1$ and i, $\mathbf{d}_{i-1}$ and $\mathbf{d}_i$, namely, $\mathbf{b}_i = \mathbf{d}_i + \mathbf{d}_{i-1} = \mathbf{r}_{i+1} - \mathbf{r}_{i-1}$ with $\mathbf{d}_i = \mathbf{r}_{i+1} - \mathbf{r}_i$ and $\mathbf{d}_{i-1} = \mathbf{r}_i - \mathbf{r}_{i-1}$. The parameter has a respective value of 1.0, 0.0, or −0.5 when one whole chain is *parallel*, *random,* or *perpendicular* to the x-axis. This parameter is usually used to discuss structural conformation and the formation of polymer chains.[52]

In short, these aforementioned structural properties would make sure possible microscopic information regarding intermolecular distance, molecular size, molecular shape, and flow alignment for sheared molecular chains under different temperatures and pressures. This is useful for a better molecular understanding into the context of variations of shear viscosities and nonequilibrium-thermodynamic states.

III. RESULTS AND DISCUSSION

The fluid of interest—*liquid n*-hexadecane—was steadily sheared with a wide range of shear rates in which the flow (x-axis) and gradient (y-axis) directional sizes, L_x and L_y, were 3.0 and 4.5 nm, respectively. Two necessary boundary conditions were set in the constant-pressure NEMD simulation box: the periodic boundary condition was adopted in *all* directions, while the Lees–Edwards boundary condition was used in the xy plane. The fluid consists of 144 n-hexadecane molecules. Note that both the melting and boiling points[45] of n-hexadecane are 289–291 and 558 K, respectively. By using the intermolecular radial distribution function curve, at various temperatures (300–500 K), the fluid was readily corroborated to exist in a *liquid* state.[18] For statistical reliability of

TABLE I. Bond length l and bond angle θ vs shear rate $\dot{\gamma}$ for n-hexadecane at 400 K and 250 MPa as obtained from *NPT*-NEMD simulation. The equilibrium value in bond length and bond angle is 0.153 nm and 109.47°, respectively.

$\dot{\gamma}$ (s^{-1})	l (nm)	θ (°)
1×10^9	0.15287	109.4598
1×10^{10}	0.15287	109.4760
1×10^{11}	0.15288	109.5725
1×10^{12}	0.15298	109.8293

data, we previously[16] validated not only rheological material function (viscosity, first and normal stress difference coefficients) but also molecular structural function (percentage of *trans* conformer, end-to-end distance, and sphericity angle) and molecular potential energy (bond stretching, bond bending, torsion, and intra- and intermolecular Lennard-Jones interactions). Using the same molecular model and state point, our data[16] fall reasonably within the predictive calculations of Berker *et al.*[6] and Chynoweth *et al.*[8]

In this article, we extended previous studies,[16–18] which have imitated the computer rheological experiment of steady state shear flow to obtain the possible microscopic picture of molecular chains undergoing structural deformation. As follows, the results were discussed in the context of both *intrinsic* and *extrinsic* structures.

A. Intrinsic structure

We employed the CM potential model in simulating n-hexadecane molecules,[8,16,45] wherein its equilibrium bond length is 0.153 nm and equilibrium bond angle is 109.47°. Below, we exhibit the degree of changes in the intrinsic structures, with respect to shear rates, by drawing on the average value of bond length and bond angle and the probability distribution of dihedral angle as well as both intra- and intermolecular radius distribution functions. Subsequently, the fluidic density in the *constant-pressure* NEMD simulation varies dramatically. Therefore, we investigate how different molecular potential energies contribute to the shear-induced change in density, which is comprised of the quasiequilibrium state plateau at low shear rates and the nonequilibrium-thermodynamic state slope at high shear rates.

1. Molecular conformation

As *NPT*-NEMD simulations were performed at 400 K and 250 MPa, the wide shear-rate range spans 3 orders of magnitude from the lowest rate of 1×10^9 s^{-1} to the highest rate of 1×10^{12} s^{-1}. Table I shows the shear-rate-induced variation in bond lengths and bond angles. At low shear rates, the length remained nearly constant and the angle approached the equilibrium angle (109.47°). In contrast to higher shear rates, the length slightly increased and approached the equilibrium length (0.153 nm), while the angle also increased but was larger than the equilibrium angle. Physically, this means that the bond length between two CH_2 groups was slightly stretched and the bond angle amongst three adjacent CH_2 groups was also widened.

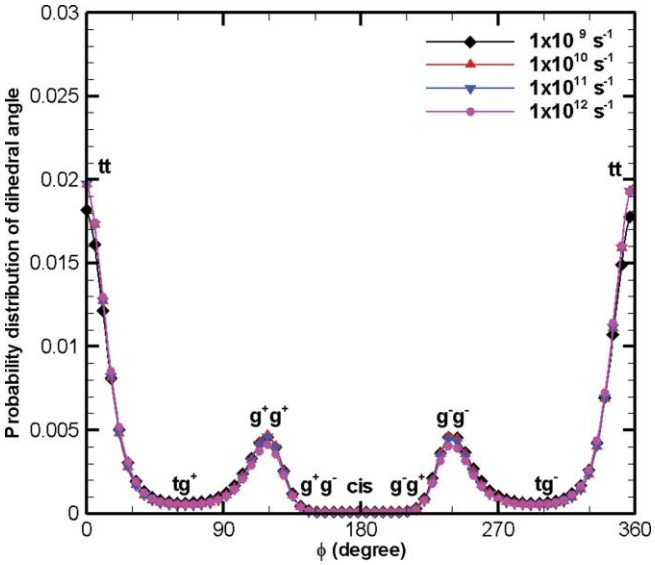

FIG. 2. Probability distribution of dihedral angle ϕ vs shear rate at 400 K and 250 MPa, as obtained from *NPT*-NEMD simulation.

To identify *miscellaneous* molecular conformations, Fig. 2 presents three stable minima states in *torsion potential energy*: the lowest energy state is the *trans* conformation, which is abbreviated tt, located at dihedral angle $\phi = 0^o$ or $\phi = 360^o$; the other two stable states are *gauche* conformations, g^+g^+ and g^-g^-, located at $\phi = 120^o$ and $\phi = 240^o$, respectively.[50]

At the lowest shear rate of 1×10^9 s^{-1} and up to 1×10^{10} s^{-1}, the *trans* conformation increased while the gauche conformation remained fixed. At medium to high shear rates, the *trans* did not vary although the gauche decreased. This variation in *trans* conformations is the same as found in related observations described by Berker *et al.*,[6] who presented the dependence of the *percentage* of *trans* conformation on shear rates for n-hexadecane molecules: they found an increase at low to medium shear rates and a subsequent plateau at higher shear rates. Up to the highest shear rate of 1×10^{12} s^{-1}, the *intensity* of the gauche peak clearly fell, whereas this peak was superimposable at low shear rates between 1×10^9 and 1×10^{11} s^{-1}.

Furthermore, the *cis* state, at $\phi = 180^o$, has a very high and unstable energy. In addition, four *intermediary* conformations are classed below: (i) tg^+ between tt and g^+g^+, (ii) tg^- between tt and g^-g^-, (iii) g^+g^- between g^+g^+ and *cis*, and (iv) g^-g^+ between g^-g^- and *cis*.[50] Consequently, we found that these *cis* and *intermediary* conformations did not vary with respect to shear rates. This finding is also similar to NEMD results of n-hexadecane undergoing elongational flow by Baig *et al.*,[15] although the flow filed is rather different.

The radial distribution function $g(r)$ is an important linkage between macroscopic thermodynamic states and microscopic intermolecular interactions within fluids. $g(r)$ describes the probability distribution for finding two molecules at a separation distance. The $g(r)$ curve involves both intramolecular and intermolecular definitions of van der

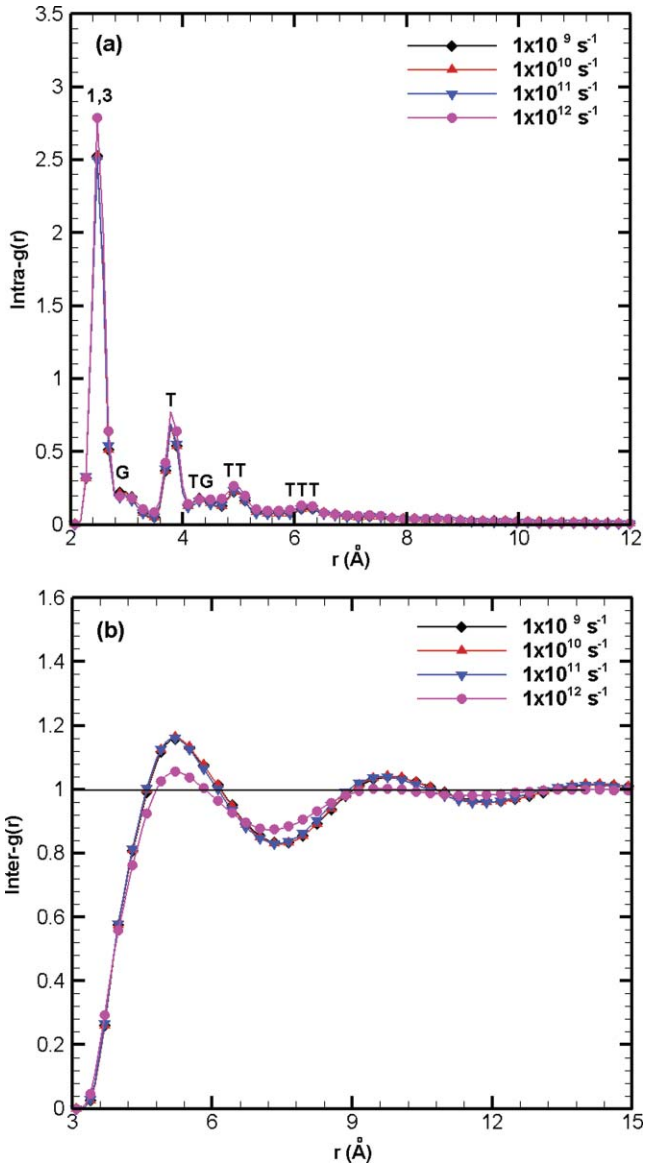

FIG. 3. (a) Intramolecular and (b) intermolecular contribution to radial distribution function vs shear rate at 400 K and 250 MPa, as obtained from *NPT*-NEMD simulation. The horizontal line indicates that the density is uniform, $g(r) = 1$.

Waals interactions, signified intra-$g(r)$ and inter-$g(r)$, respectively. The intra-$g(r)$ curve shows a molecular chain's various conformations, including *trans* and *gauche*. The inter-$g(r)$ curve can distinguish a pure material's phase states: gas, liquid, and solid.[49]

Figure 3 illustrates both intra-$g(r)$ and inter-$g(r)$ curves at different shear rates. As shown in the intra-$g(r)$ curve, the maximum peak indicates that the 1,3 distance is associated with the bond angle among three adjacent CH_2 groups. Within this distance, notably, the van der Waals interaction does not take place. The *G* peak occurring at 2.88 Å is the 1,4 distance in a gauche bond among four adjacent CH_2 groups and the *T* peak was its *trans* counterpart at 3.79 Å. In the 1,5 distance, the *TG* peak was found at 4.30 Å with one gauche bond and one *trans* bond, and the *TT* peak at 4.90 Å with two *trans* bonds. The *TTT* peak was labeled at 6.12 Å in the 1,6 distance with three *trans* bonds. Notably, this intra-$g(r)$ curve is in the excellent agreement with MD results of polyethylene (PE) studied by Pant and Boyd.[54] Except for the 1,3 peak, we must attempt variation in the other five peaks/conformations with respect to shear rates. As a result, these curves almost overlay each other. Up to the highest shear rate of 1×10^{12} s^{-1}, only the *T* peak's strength rose slightly. This means that the probability of the *single trans bond* increased.

Moreover, the inter-$g(r)$ curves at short distances ($r < 3.08$ Å) approached zero because of strong repulsive forces. The first and largest peak occurred at $r \approx 5.21$ Å. This local maximum indicates that the probability of finding a pair of CH_2 groups with such a separation was highest when the pair potential energy was at a *minimum*. The inter-$g(r)$ curve then fell and passed through a minimum value at $\sim r \approx 7.43$ Å. The chances of finding a pair of molecules were lower and potential energy also reached a *maximum* value. Finally, at larger separations (passing through the second peak of 9.76 Å), the potential energy approached *zero* with some fluctuation, so that the density was uniform, i.e., $g(r) \approx 1$.[55] As a whole, the shapes of the inter-$g(r)$ curves described above were clearly liquid state characteristics in accordance with McQuarrie's treatise of statistical mechanics.[56] Also, the curves were in good agreement with the studies of Tsuchiya *et al.*,[49] who predicted the melting point of *n*-alkanes by using equilibrium molecular dynamic (EMD) simulations. These curves shown in Fig. 3(a) almost did not vary from 1×10^9 to 1×10^{11} s^{-1}. Up to the highest shear rate of 1×10^{12} s^{-1}, the *intensity* of the inter-$g(r)$ curve's first peak fell, while the curves occurring at longer distances ($r > 10.0$ Å) tended to gradually approach a value of *1*. This description implies that at low shear rates, the intermolecular distance remains almost unchanged while it is lengthened at extreme shear rates. We noticed that these variations in $g(r)$ curves above were the same as those observed in the NEMD simulations described by Bosko *et al.* for a dendrimer.[28] In addition, Marcelli *et al.*[57] demonstrated that the intensity of the first peak in the $g(r)$ curves at an extreme shear rate was specifically lower than that obtained at an equilibrium state. Previously, we presented[18] the inter-$g(r)$ curve's dependence on thermodynamic state variables: the intermolecular distance strongly increased with rising temperature, whereas the distance shortened by increasing either pressure or density.

Notably, we might cautiously suggest that in the context of all of the data related to the values aforementioned from lowest shear rate of $1 \times 10^9 s^{-1}$ to the highest shear rate of $1 \times 10^{12.0}$ s^{-1}, the degree of change was minimal at less than about 0.3% as a whole. Therefore, this observation indicates that the intrinsic structures, which include bond length, bond angle, molecular conformation, and intermolecular distance, exhibit small variations according to shear rate (with the exception of extreme shear rates).

2. Molecular potential

In Sec. III A 1, we previously proposed that when a chain was aggressively sheared, its intrinsic structures changes minimally according to shear rate. We

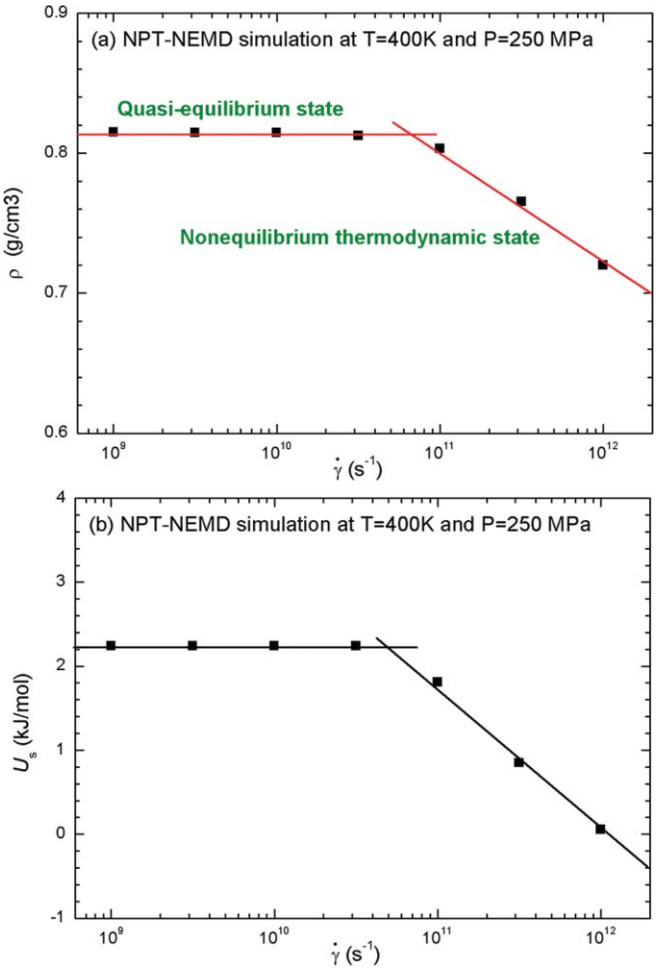

FIG. 4. (a) Density ρ and (b) bond stretching potential energy U_s vs shear rate $\dot{\gamma}$ at 400 K and 250 MPa, as obtained from *NPT*-NEMD simulation. The drawn lines are fit to the data.

drew further on *a potential energy representation* with respect to shear rate: bond stretching, bond bending, torsion, and intra- and intermolecular Lennard-Jones (or van der Waals) interactions. This is useful in observing how the evident variation in these molecular potentials contributes to our understanding of the effect of shear rate on density.

In Fig. 4(a), we present the nonequilibrium-thermodynamic state curve in *NPT*-NEMD simulations at 400 K and 250 MPa, namely, the density–shear rate ($\rho - \dot{\gamma}$) curve, where two lines are drawn to fit to the data. The density rather dramatically varies with increasing shear rates. Clearly, one transition point occurred at about $\dot{\gamma} = 1 \times 10^{11}$ s^{-1}. Before the transition point, the density almost remained nearly constant, about $\rho_{ne} = 0.814$ g/cm^3. Previously, we obtained the equilibrium state curve of pressure against density under isothermal conditions of 400 K.[16] The equilibrium density is $\rho_e = 0.801$ g/cm^3 at 400 K and 250 MPa. Thus, we found that ρ_{ne} were slightly larger than ρ_e. Rah and Eu[58] discussed the effect of shear flow on a nonequilibrium liquid–vapor interface system; their results revealed that the liquid phase side density is also slightly increased, relative to the equilibrium density. Thereby, in Fig. 4(a), the convergent density appears at the quasiequilibrium state.

Note that, for rheological behaviors of non-Newtonian fluids, the variation in viscosity with respect to shear rate is classified into two categories: shear thinning (thixotropic) and shear thickening (dilatant).[36,59] When the viscosity decreases with increasing shear rate, the liquid is called thixotropic. However, the viscosity can increase with increasing shear rate. Then the liquid is called dilatant. As evident from Fig. 4(a), in the case of the shear thinning or thixotropic *n*-hexadecane fluid, the density rapidly decreased with increasing shear rate. We may suggest that this $\rho - \dot{\gamma}$ relationship at high shear rates is known as a *decrease in density* or *volume dilation* phenomenon of a *nonlinear* nonequilibrium-thermodynamic state behavior.[7,16,18] Therefore, below we would generalized the effect of shear thinning on variations of fluid density, molecular structural property, and potential energy with respect to shear rates.

In passing, we previously discussed[16] the effects of temperature and pressure on the slope of the nonequilibrium-thermodynamic state behavior: the degree of NTS behavior increased linearly as temperatures increased and decreased as pressure increased. Significantly, the tendency toward variation of the degree of shear thinning in rheology was qualitatively *contrary* to that of the NTS behavior in thermodynamics. As regards NEMD results of the decane, hexadecane, and tetracosane liquids, Cui *et al.*[9] saw that the NTS behavior is not related to chain length.

Figure 4(b) shows the variation in bond stretching potential energy with respect to shear rates ($U_s - \dot{\gamma}$). Surprisingly, the transition point was also found at about $\dot{\gamma} = 1 \times 10^{11}$ s^{-1}. Before this point, the stretching energy tended toward the convergent value. Beyond the point, however, the bond stretching energy clearly decreased. This is due to the fact that, before the transition point, the bond length was held constant; whereas beyond the transition point, the bond length with increasing shear rates approached equilibrium, as shown in Table I. Overall, the shear-rate dependence of stretching potential energy is similar to that of density.

To augment our understanding of molecular interactions contributing to variation in density, we plot the bond bending and torsion potential energies (U_b and U_t) as a function of shear rate in Fig. 5. As expected, the transition point also occurred at about $\dot{\gamma} = 1 \times 10^{11}$ s^{-1}. In addition, at low shear rates, both energies remained approximately constant, wherein the bending energy converged at zero due to the bond angle approaching the equilibrium angle. Beyond the transition point, both energies increased with shear rate in which the bond angle was widened and was larger than the equilibrium angle, while the probability of *trans* and gauche conformations increased and decreased, respectively. Such a tendency is in opposition to the variation in density and stretching energy (cf. Fig. 4).

Moreover, the intra- and inter-LJ potential energies (intra-U_{LJ} and inter-U_{LJ}) are graphed as a function of shear rate in Fig. 6. The variation in intra-U_{LJ} and inter-U_{LJ} is same with that in U_b and U_t (cf. Fig. 5). Before the transition point occurring at about $\dot{\gamma} = 1 \times 10^{11}$ s^{-1}, the intra-U_{LJ} and inter-U_{LJ} did not depend on shear rate, whereas those energies also increased with shear rate due to the increase in the probability of the intramolecular *trans-bond* and the distance

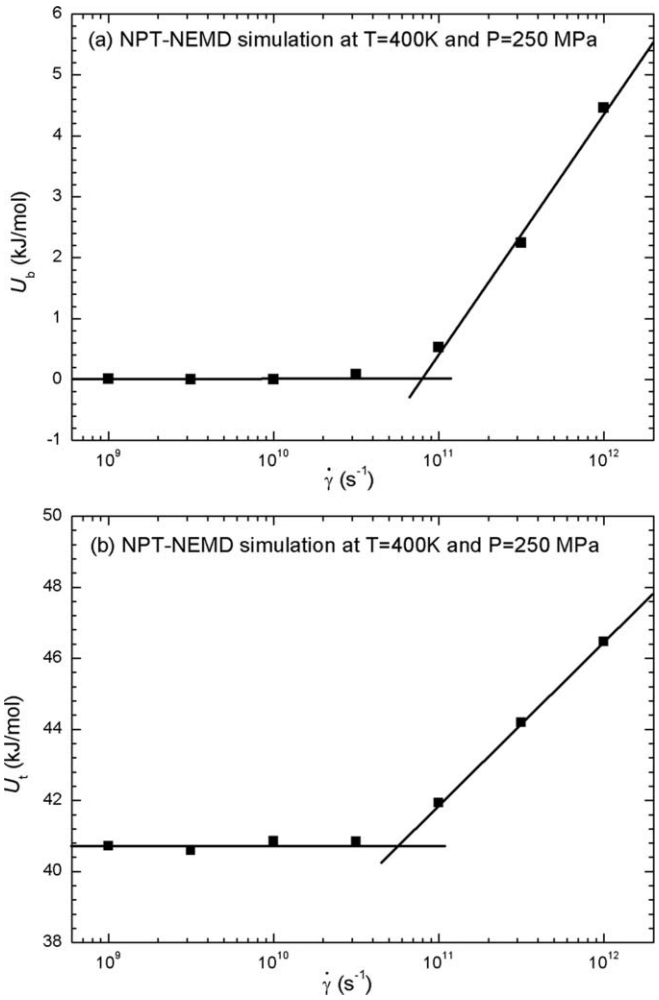

FIG. 5. (a) Bond bending U_b and (b) torsion U_t potential energies vs shear rate at 400 K and 250 MPa, as obtained from *NPT*-NEMD simulation. The drawn lines are fit to the data.

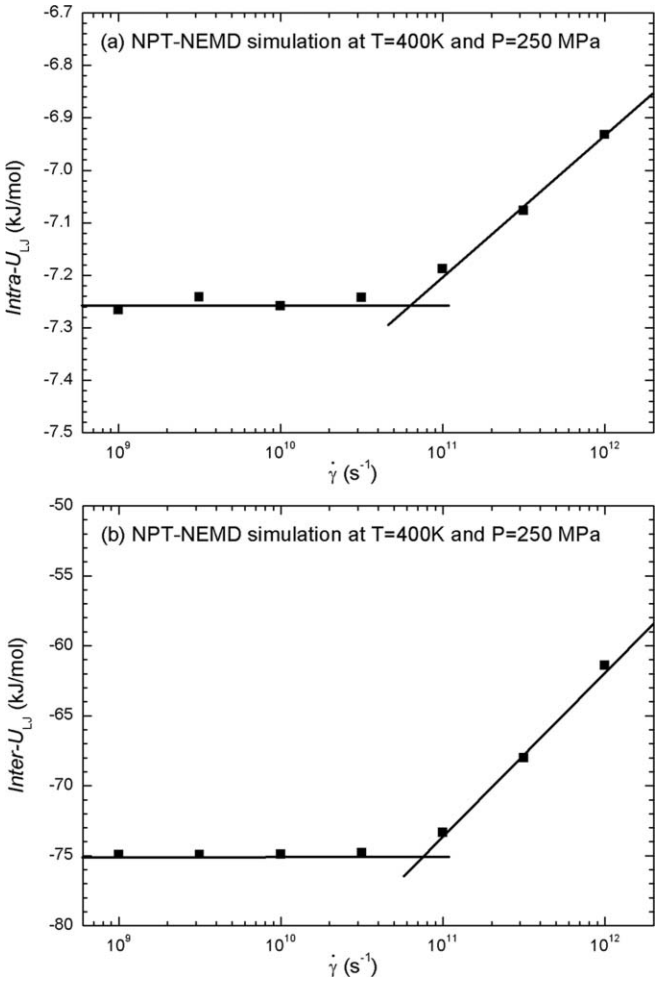

FIG. 6. (a) Intra- and (b) inter-Lennard-Jones potential energies U_{LJ} vs shear rate $\dot{\gamma}$ at 400 K and 250 MPa, as obtained from *NPT*-NEMD simulation. The drawn lines are fit to the data.

of intermolecular separation. Note that, at low shear rates, all potential energies are equal to the convergent values because the sheared fluidic density approaches equilibrium.

Returning to Fig. 4(a), the convergent density is 0.814 g/cm^3 and the highest-shear-rate density is 0.720 g/cm^3. This change in density is about 11.5%. It is worth mentioning how these potential energies, U, significantly contribute to the nonequilibrium-thermodynamic state behavior—the decrease in density is associated with increasing shear rate. At this point, we can simply define a change in potential energy, ΔU, as follows:

$$\Delta U = U_H - U_C, \tag{6}$$

where U_H is the highest-shear-rate potential energy, $U(\dot{\gamma} = 1 \times 10^{12}\ \mathrm{s}^{-1})$, and U_C is the convergent potential energy, $\bar{U}(\dot{\gamma} < 1 \times 10^{11}\ \mathrm{s}^{-1})$. Note that the value of U_C is determined by the least-square method fitting the data.

Table II lists the values of $U(\dot{\gamma} = 1 \times 10^{12}\ \mathrm{s}^{-1})$, $\bar{U}(\dot{\gamma} < 1 \times 10^{11}\ \mathrm{s}^{-1})$, and ΔU resultant from various molecular interactions. By calculating the absolute magnitude of ΔU, we can obtain the order of contributor from the largest to the smallest: inter-LJ, torsion, bending, stretching, and intra-LJ interactions. Therefore, we might suggest a physical justification such that when the nonequilibrium-thermodynamic density of sheared molecular fluids is taken from the near equilibrium plateau following to the slope of nonequilibrium-thermodynamic state regime, the maximum contributor (62%) is the inter-LJ, the second (26%) is the torsion, and the minimum (2%) is the intra-LJ. In summary, at low shear rates, the nonequilibrium states of molecular fluids tend to be the quasiequilibrium ones, while their intramolecular structures/conformations and intermolecular distances remain unchanged. In contrast, high shear rates

TABLE II. The convergent value $\bar{U}(\dot{\gamma} < 1 \times 10^{11}\ \mathrm{s}^{-1})$, the highest-shear-rate value $U(\dot{\gamma} = 1 \times 10^{12}\ \mathrm{s}^{-1})$, and the change ΔU in potential energy for various interactions of *n*-hexadecane at 400 K and 250 MPa, as obtained from *NPT*-NEMD simulation. The unit of potential energy is kJ/mol.

Interaction	$\bar{U}(\dot{\gamma} < 1 \times 10^{11}\ \mathrm{s}^{-1})$	$U(\dot{\gamma} = 1 \times 10^{12}\ \mathrm{s}^{-1})$	ΔU
Bond stretching	2.240	0.053	−2.187
Bond bending	0.023	4.458	4.435
Torsion	40.817	46.468	5.652
Intra-Lennard-Jones	−7.252	−6.932	0.320
Inter-Lennard-Jones	−74.883	−61.415	13.467
Total of potentials	−39.055	−17.368	21.686

cause an increase in bond length and bond angle such that the fully stretched chain may be seen as a very stiff chain with a *zigzag* shape, wherein the probability of *trans* and gauche conformations increases and decreases, respectively.[50]

Numerous constant-volume NEMD studies[15,25,27] have discussed nonequilibrium-thermodynamic pressures inducing the change in various molecular potential energies and have come to a significant conclusion: variation of pressure along with shear rate is related to the intermolecular LJ potential. Thus, our analysis above is in agreement with their results. Previously, we proposed[18] that the probable cause of the nonequilibrium-thermodynamic state behavior in NEMD simulations was related to the imposed shear rate and the root mean square molecular velocity.

B. Extrinsic structure

Through analyzing the extrinsic structure deformation of molecules, this second investigation is performed to understand the molecular origin of shear flow behavior and exhibit three points of fact: molecular size, molecular appearance as well as flow alignment as quantified by the squared radius of gyration, the sphericity angle, and the orientational order parameter, respectively. The dramatic variations in these structure properties, with respect to shear rates, are further examined as a function of temperature and pressure. At the same time, we propose a plausible justification for which the insightful change of shear viscosity and density depends on the structural properties.

1. Molecular dimension

Two common parameters are used to monitor the molecular chain size: the square end-to-end distance R^2 and the square radius of gyration $R_g{}^2$. To initially verify the reliability of data regarding the average size of *n*-hexadecane molecules, occurring at an equilibrium state point of 477.6 K and 0.896 g/cm^3, we calculated that the average value of R^2 was 175 Å^2 and was close to the predictions (177± 4 Å^2) of Chynoweth *et al.*[8] Furthermore, at a *liquid* state point of 372 K and 0.719 g/cm^3, our R^2 and $R_g{}^2$ values were 200 and 24.5 Å^2, respectively. Then, we can also obtain that the $R^2/R_g{}^2$ ratio is 8.16 and a non-Gaussian chain due to the ideal Gaussian chain's $R^2/R_g{}^2 = 6$. These values are reasonable and fall within the estimated values of Goo *et al.*,[60] who used EMD simulations to discuss the diffusion behavior of various *n*-alkanes (C_{12}–C_{44}).

We further presented the variation in $R_g{}^2$ with respect to shear rate. This is helpful in understanding a deformation history of molecular chains flowing in the shear flow field. Figure 7 shows $R_g{}^2$ plotted against shear rate at varying temperatures and pressures. Roughly, one transition point occurred at about $\dot{\gamma} = 1 \times 10^{11}$ s^{-1}. This point also found in variation of the density and the molecular potential mentioned above (cf. Figs. 4–6). Henceforth, a vertical dash line in figures is illustrated at the transition point.

Before the transition point, $\dot{\gamma} < 1 \times 10^{11}$ s^{-1}, $R_g{}^2$ slightly increased with the shear rate. Physically, this behavior may be attributed to the shear-induced stretching deformation of molecular chains, wherein the fluidic density is almost held constant such that the molecular motion has hardly changed. Beyond the transition point, $\dot{\gamma} > 1 \times 10^{11}$ s^{-1}, as the density rapidly fell, a surprisingly decrease of $R_g{}^2$ implied that the chains spontaneously shrink during shear flow. It has also been seen in previous NEMD literature of *n*-alkane fluids[7,9,10,12,31,39,51] that the reverse trend of $R_g{}^2$ was found at higher shear rates, whereas at very low shear rates, the $R_g{}^2$ value tended toward the equilibrium value. Generally, the *n*-hexadecane molecular chain is in the gauche conformation under equilibrium liquid state. Under shear flow, the chain is probably straightened. To rationalize the interesting decrease in $R_g{}^2$, Padilla and Toxvaerd[61] suggested the following interpretation of a competition between two mechanisms: the alignment of chains dominated at low shear rates and the deformation of chains dominated at high shear rates. According to the same discussions for NEMD simulations of *n*-hexadecane molecules, Khare *et al.*[10] obviously indicated that at low shear rates, chains were stretched and tended to line up with the flow, while at very high shear rates they

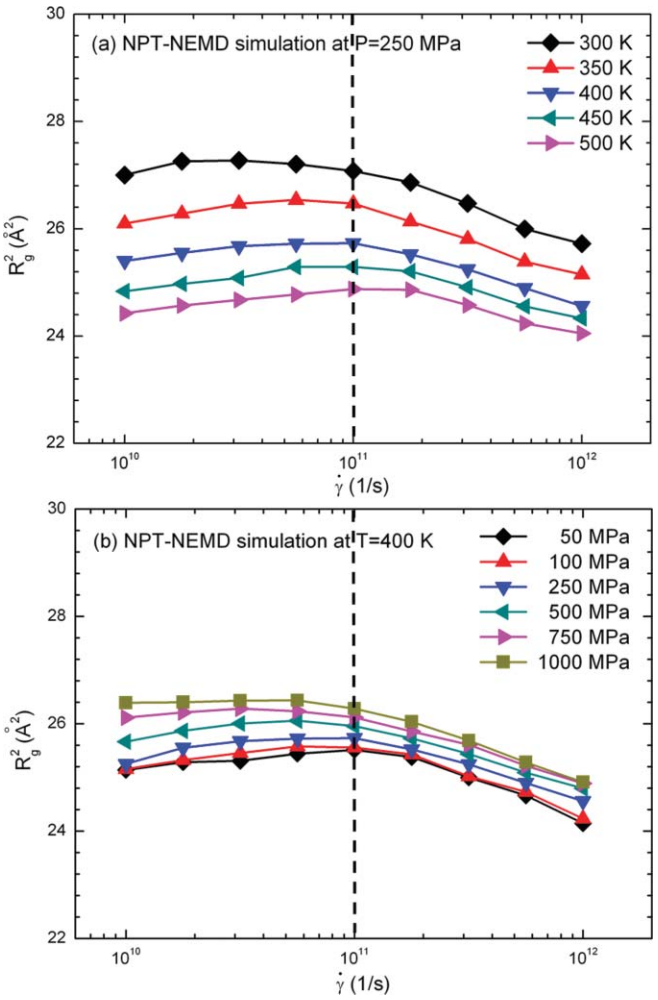

FIG. 7. Squared radii of gyration R_g^2 vs shear rates $\dot{\gamma}$ (a) at 250 MPa and various temperatures between 300 and 500 K and (b) at 400 K and various pressures between 50 and 1000 MPa, as obtained from *NPT*-NEMD simulations. The vertical dash line indicates a transition point at a particular shear rate, $\dot{\gamma} = 1 \times 10^{11}$ s^{-1}.

tumbled more frequently and tended to be coiled. In a significant experimental observation, single-polymer dynamic in steady shear flow was found by Smith *et al.*,[62] who demonstrated the stretch and tumble motions of the chains with respect to shear rates.

Some NEMD simulations of long chains have included linear, branch, and dendrimer structures.[14,25,27,32,63,64] However, they clearly exhibited an increased value of R_g^2 at high shear rates. Thus, we might speculate whether or not the tumble of the chain is related to the chain length; viz., the decrease in R_g^2 depends on chain length. This conclusion was also proposed by Cui *et al.*,[9] who discussed rheological properties of normal decane, hexadecane, and tetracosane liquids by using NEMD simulations.

According to the general understanding of polymer physics,[36,53] long chains are subject to *entanglement*. Notably, the degree of entanglement (DOE) of short chains is relatively low. From this point, we have further proposed that the likelihood that the chain might tumble depends on the DOE. In other words, the sheared short chain lightly *disentangles* at low shear rates. Then, approaching higher shear rates, the chain almost *disentangles* and naturally *shrinks* to tumble with a decrease in its size. Due to a high DOE, the long chain under shear is stretched while it does *not* easily disentangle; specifically, this shows an increase in R_g^2, which implies that the chain tumbled with hardness.

Regarding entanglemental characteristic of molecules, Foteinopoulou *et al.*[29] demonstrated that once the length of a chain was larger than about 200 united atoms, the chain began to become entangled. From short to long linear chain molecules, Kröger and Hess[24] built the *finite extensible nonlinear elastic* chain motion to analyze the relationship between the zero-shear-rate viscosity (η_0) and the molecular length (N). Consequently, the η_0–N relationship clearly represents a critical chain length characterizing the crossover point from $\eta_0 \propto N^1$ of the Roused model to $\eta_0 \propto N^{3.0-3.5}$ of the reptation model. This crossover was obtained for chain lengths of the order of 100 monomers. $N > 100$ is considered to be a reasonable phenomenological description of entangled polymer melts. Therefore, in our simulation, the dramatic variation in R_g^2 reflects the notion that the n-hexadecane molecule may relatively be quite short and very stiff with a little entanglement.

Returning to Fig. 7(a), the R_g^2 value evidently decreases as the temperature gradually rises from 300 to 500 K. This is due to the temperature increase, the decrease in density, and the increase in volume which allows the free space of molecular motion to be expanded while the molecular chain spontaneously shrinks itself. As regards the n-hexadecane under the isothermal conditions of 400 K, its state curve of density plotted against temperature can be referred to in our previous study.[16]

Such a temperature-induced variation in R_g^2 is in good agreement with the EMD results of Goo *et al.*,[60] who compared the diffusion behavior of various *liquid* n-alkanes. In addition, Fujiwra and Sato[52] simulated the structural formation of a single PE chain with 500 repeat-units from the lowest temperature (100 K) of the orientationally ordered structure to the extreme temperature (800 K) of the random coil structure. As the temperatures T continuously rose, their observations showed that three features: (i) below the glass-translation temperature (T_g) about 400 K, the PE chain is a solid state and its R_g^2 value is held constant; (ii) $T_g < T < 550$ K, the PE chain is at a melt state and its R_g^2 value clearly decreases; and (iii) at high temperatures ($T > 550$ K), R_g^2 increased instead.

As for experimental evidence, Hajduk *et al.*[65] studied the disordered phase of block copolymer *melts* that obtained a decrease and increase in R_g^2 with increasing temperature and pressure, respectively. Earlier, in order to better understand the squared end-to-end distance R^2 depending on the temperature T of PE *melt*, Ciferri *et al.*[66] employed a method for determining temperature coefficient, i.e., $d\ln(R^2)/dT$, which can contribute important information regarding the chain configuration. Their result demonstrated that $d\ln(R^2)/dT < 0$ implied a decrease in R^2 with increasing temperature. Notably, with respect to molecular interactions in *dilute polymer solutions*,[67,68] when the temperature is larger than the *theta* temperature (T_θ), the polymer chain's R_g^2 increases, wherein T_θ is defined at which time the coiled polymer chains expand to their full contour lengths and become rod-shaped. Also T_θ is usually known as the Flory temperature.[68]

Figure 7(b) indicates that the R_g^2 value increases as the pressure increases over a wide range from 50 to 1000 MPa. This is also similar to the experimental observation of Hajduk *et al.*[65] Note that our constant-pressure NEMD system treated the change in volume that corresponds to the change in the size of the periodic boundary condition of the z-direction, wherein the flow (x-axis) and gradient (y-axis) directional sizes are held constant. Therefore, the increase in R_g^2 is due to the pressure increase which causes the decrease in volume. Referring to our prior study,[16] we presented the thermodynamic state curve of pressure versus density in n-hexadecane under the isothermal condition of 400 K. Then, the free space of molecular motion is compressed in the z-direction which causes one chain to be forcedly extended around other chains. As a whole, our shear rate, temperature, and pressure induced variations in R_g^2 for liquid n-hexadecane qualitatively match the results of the abovementioned reviewed literature. Eventually, we also attempted to show that the $dR_g^2/d\dot{\gamma}$ slope, whether occurring before or beyond the transition point, did not significantly vary with respect to temperature and pressure.

2. Molecular appearance

A more detailed understanding of molecular conformations requires an investigation regarding appearance characteristics through the sphericity angle φ. At equilibrium, the shape of chains is going to be perfectly spherical, i.e., $\varphi = 45°$. This value also implies that fluids follow Newtonian behavior.[6] Therefore, under shear, the shape seems to be ellipsoidal with $\varphi < 45°$.

Under different temperatures and pressures, Fig. 8 displays the changes in φ with respect to shear rates. Note that a vertical dash line given in the figure indicates a particular shear rate at $\dot{\gamma} = 1 \times 10^{11}$ s^{-1}, namely, the aforementioned transition point of nonequilibrium-thermodynamic state curve

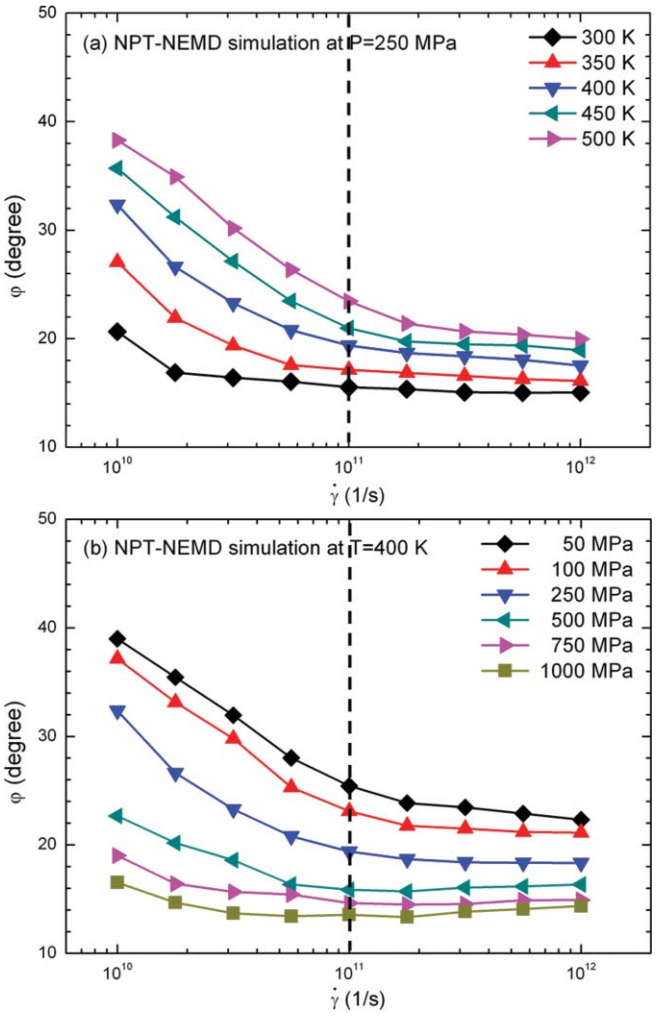

FIG. 8. Sphericity angles φ vs shear rates $\dot{\gamma}$ (a) at 250 MPa and various temperatures between 300 and 500 K and at (b) 400 K and various pressures between 50 and 1000 MPa, as obtained from *NPT*–NEMD simulations. The vertical dash line indicates a transition point at a particular shear rate, $\dot{\gamma} = 1 \times 10^{11}$ s^{-1}.

depicted in Fig. 4(a). At low shear rates, $\dot{\gamma} < 1 \times 10^{11}$ s^{-1}, the value of φ strongly decreased with increasing shear rates. Thus, this physical picture signifies that the shape is an increasingly sharper ellipsoid. As a whole, our observation is in good agreement with the results of Berker *et al.*[6] and Chynoweth *et al.*[8] According to our physical understanding of *entangled* polymer chains, φ is inversely related to R_g^2. As shear rate increases, an increase in R_g^2 causes the overall shape to become increasingly sharper ellipsoid. Furthermore, Fig. 8(a) shows that the φ value is enhanced when the temperature rises. In Fig. 8(b) the value decreases in reaction to increased pressure. We might suggest that such changes in the φ value also are attributed to R_g^2: the R_g^2 value decreases with increasing temperatures and increases with increasing pressures (cf. Fig. 7).

When the shear rate was increased to over 1×10^{11} s^{-1}, we observed that the value of φ did not significantly vary, i.e., the rate of change in φ with $\dot{\gamma}$ approached zero, $d\varphi/d\dot{\gamma} \approx 0$. In other words, the shape of the molecule remains a fixed sharp ellipsoid. We may interpret that at high shear rates, the chains nearly *disentangle* and possibly *slide*. Also, Cui *et al.*[9] suggested that especially for the case of higher shear rates, the dominant motion between the chains was the sliding behavior. In experimental observation, Boukany *et al.*[69] found the *interfacial stick–slip transition* of entangled 1,4-polybutadiene and polyisoprene melts in simple shear by using a specially designed controlled-force shear rheometer.

Connecting the changes in R_g^2 and φ before the transition point, the size of chains increased slightly and their shape approached an increasingly sharper ellipsoid. Beyond the transition point, the size greatly decreased and the appearance became a sharper ellipsoid with a finite value of φ. Additionally, at high temperatures or low pressures, the chains easily formed a tendency toward a random coil with a small R_g^2, whereas the chain approached a sharper ellipsoid with a large R_g^2. Moreover, we found that before the transition point, the $d\varphi/d\dot{\gamma}$ slope obviously increased with increasing temperature, while one decreased with increasing pressure. Beyond the transition point, we found that φ plateau, i.e., $d\varphi/d\dot{\gamma} \approx 0$, regardless of temperature or pressure. Thereby, the sphericity angle can well parametrize and help us to understand changes in the chain's shape during shear flow.

3. Molecular orientation

One quantity of the structural order is the orientation of molecular chains along the flow direction. The orientational order parameter S_x signified the degree of orientation along the x-axis for an individual molecular chain.[52] If the chains are parallel, random, or perpendicular to the x-axis, S_x equals a value of 1.0, 0.0, and −0.5, respectively. Such a parameter is always applied in discussions of polymer chains in regard to structural conformations.[52]

Figure 9 shows the effects of temperature and pressure on the changes in S_x with respect to shear rates, wherein a vertical dash line signifies a transition point at a particular shear rate, $\dot{\gamma} = 1 \times 10^{11}$ s^{-1}. Before the transition point, the values of S_x greatly increased with increasing shear rates; this S_x variation is opposite to the φ variation (cf. Fig. 8). Beyond the transition point, the S_x values were almost insensitive to the variation of shear rate, namely, $dS_x/d\dot{\gamma} \approx 0$. This tendency is the same with the φ variation. Furthermore, in macroscopic simulations, Tucker and co-workers[70–72] predicted variations in orientation of fibers under both shear and elongation flows, which are in agreement with related experimental observations. Therefore, our microscopic simulations of molecular orientation are similar to their results: as the shear rate continuously increases, the degree of orientation of the chain along the flow direction simultaneously increases and eventually approaches a limitative value.

Such a result is also close to variations in the alignment angle found in related NEMD investigations.[9,11,12,25,27] This change in flow orientation is attributed to the sheared short chains becoming slightly *disentangled* at low shear rates; at high shear rates, the whole chains are almost completely disentangled.

As shown in Fig. 9(a), the value of S_x decreases with rising temperatures. This is because, as the temperature

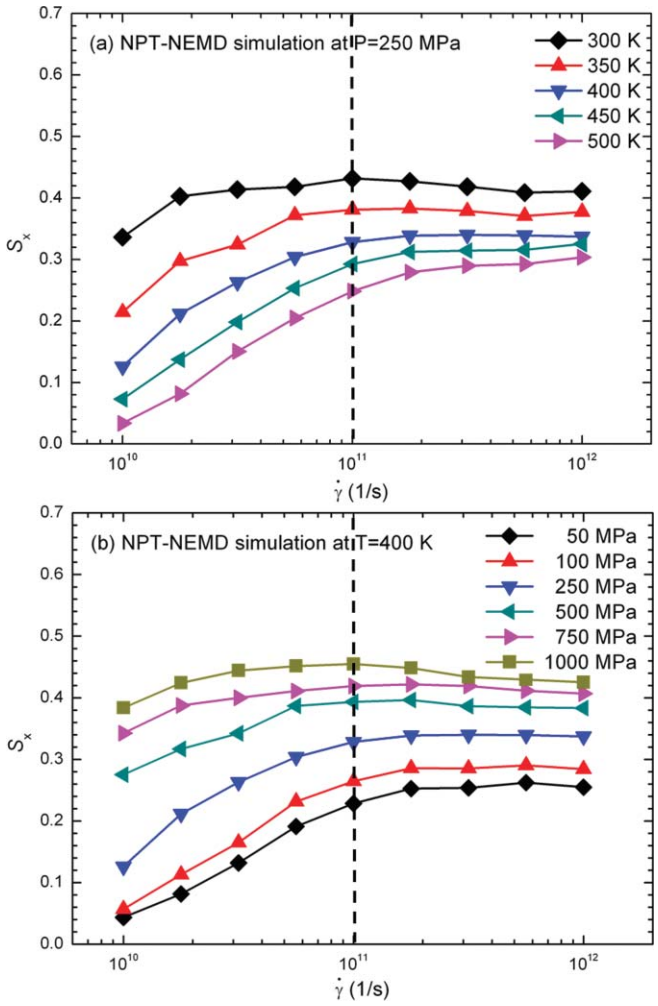

FIG. 9. Orientational orders S_x (a) at 250 MPa and various temperatures between 300 and 500 K and (b) at 400 K and various pressures between 50 and 1000 MPa, as obtained from *NPT*–NEMD simulations. The vertical dash line indicates a transition point at a particular shear rate, $\dot{\gamma} = 1 \times 10^{11}$ s^{-1}.

increases, there is an increase in the free space of molecular motion while the molecular chain spontaneously shrinks itself to become the *random coil*. In Fig. 9(b), the value of S_x increases as the pressure increases. Because of this, the free space of the molecules is correspondingly compressed, causing one chain to be forcedly extended around other chains to effectively enhance the orientational order along the flow direction. Moreover, before the transition point, the slope $dS_x/d\dot{\gamma}$ obviously increased with increasing temperature and decreased with increasing pressure. Beyond the transition point, the convergent S_x value plateau or $dS_x/d\dot{\gamma} \approx 0$ was found, and no change was affected by either temperature or pressure. This tendency is also similar to prior observations of the sphericity angle (cf. Fig. 8).

For a more comprehensive survey, we present previous discussions[16,18] based on radial distribution function about variations of the intermolecular distance with respect to the shear rates, temperatures, and pressures. At low shear rates, the RDF curves bore almost no relation to the shear rate. Thus, the intermolecular distance is held almost constant. In contrast, at high shear rates, the intensity of the first and highest peaks in the RDF curves fell with an increasing shear rate. This situation provided evidence for an increase in the intermolecular distance. Moreover, with rising temperatures, the RDF curves revealed increases in intermolecular distances. On the other hand, upon increasing either pressure or temperature, we found that the intermolecular distance shortened. Furthermore, the overall characteristics of the RDF curves showed our research fluid existing in the liquid state.

Finally, we briefly summarize with some significant remarks describing the *molecular physical picture* for sheared *n*-hexadecane molecules with respect to temperatures and pressures. At low shear rates, the molecules are slightly elongated, while their shape becomes increasingly ellipsoidal and the flow-orientational-order increases. At high shear rates, they are strongly contracted and both their shape and order are held almost constant. On the one hand, as the temperature rises, the molecules are more likely to occur at a random coil state and have their size and order decrease. On the other hand, one can expect that when the pressure is increased, the size and order increase but the shape becomes a sharper ellipsoid.

IV. CONCLUSION

The isobaric–isothermal nonequilibrium molecular dynamic (*NPT*-NEMD) simulations were used to investigate the macroscopic shear flow behavior via the accompanying changes in microscopic structures. The fluid of interest is *liquid n*-hexadecane molecules. In the case of the shear thinning or thixotropic *n*-hexadecane fluid, we discussed variations of molecular structural properties and potential energies with respect to shear rates. Although the molecules are aggressively exerted upon shear deformation, their intrinsic structure hardly changes, except in the case of extreme shear rates.

It is important to note that, with respect to shear rates, molecular potential energies are related to the nonequilibrium-thermodynamic state curve. Regarding the shear-induced variation in extrinsic structural properties, the molecular size and its appearance are determined by using the squared radius of gyration and the sphericity angle, respectively. In addition, the orientational order can quantify the molecular degree of orientation along the flow direction. Interestingly, we propose that those three structural parameters are connected in response to the thermodynamic state variable of density and the rheological material function of shear viscosity.

At low shear rates, $\dot{\gamma} < 1 \times 10^{11}$ s^{-1}, the fluid approaches Newtonian behavior with zero-shear-rate viscosity, while its density tends toward equilibrium. As regards microscopic observation, molecular potential energies clearly approach the convergent values, which include bond stretching, bond bending, torsion, and intra- and intermolecular distances of van der Waals interactions. Simultaneously, the intermolecular distance of separation is held nearly constant. Furthermore, the molecules are somewhat elongated, while they entirely become an increasingly sharp ellipsoid with the higher order along flow direction.

In contrast to high shear rates, $\dot{\gamma} > 1 \times 10^{11}$ s^{-1}, the nonequilibrium-thermodynamic state slope—a decrease in

density with increasing shear rate—may be attributed to molecular interactions. From the plateau of quasiequilibrium following the slope of nonequilibrium-thermodynamic state, the maximum contributor is the intermolecular LJ potential, the second is the torsion potential, and the minimum is the intramolecular LJ potential. In a response to rheological behavior, the shear thinning occurs in a reduction of shear viscosity with an increasing shear rate. Significantly, the whole molecular picture shows that the molecules strongly contract and tumble and their shape and order remain almost unchanged. Additionally, there is an increase in the intermolecular distance.

In many practical applications whether or not the high/low shear-rate situation is observed, such as spreading, wetting, lubrication, friction, and polymer coating and processing, an in-depth understanding of ultrathin films sheared in a wide range of shear rate is of importance at the nanolevel. Therefore, NEMD simulations can provide valuable thermodynamics and rheological information to research a particular relationship between macroscopic transport phenomena and microscopic molecular interactions, especially for unexpected behavior and properties of molecularly thin films.

Specifically, we also point out that these properties are sensitive to the variation of temperature and pressure. The temperature increases and causes a decrease in the fluid's density and viscosity, while the molecular appearance is close to a random coil with a decrease in its size; as well, the order correspondingly falls. Moreover, the intermolecular distance is correspondingly lengthened. One can expect that when the pressure increases, the size and the order increase, but the shape becomes an increasingly sharp ellipsoid. Also, the intermolecular distance is shortened. This situation obtains evidence of an increase of viscosity and density.

ACKNOWLEDGMENTS

We thank the National Science Council of the Republic of China for financial support (Grant No. NSC98–2221-E-007–008-MY2) and CoreTech System Co., Ltd (Moldex3D).

[1]D. J. Evans and G. P. Morriss, Comput. Phys. Rep. **1**, 297 (1984).
[2]D. J. Evans and G. P. Morriss, *Statistical Mechanics of Nonequilibrium Liquids* (Cambridge University Press, Cambridge, 2008).
[3]A. W. Lees and S. F. Edwards, J. Phys. C **5**, 1921 (1972).
[4]D. J. Evans, Phys. Rev. A **23**, 1988 (1981).
[5]D. J. Evans and G. P. Morriss, Phys. Rev. Lett. **56**, 2172 (1986).
[6]A. Berker, S. Chynoweth, U. C. Klomp, and Y. Michopoulos, J. Chem. Soc., Faraday Trans. **88**, 1719 (1992).
[7]P. J. Daivis and D. J. Evans, J. Chem. Phys. **100**, 541 (1994).
[8]S. Chynoweth, R. C. Coy, and Y. Michopoulos, Proc. Inst. Mech. Eng., Part J: J. Eng. Tribol. **209**, 243 (1995).
[9]S. T. Cui, S. A. Gupta, P. T. Cummings, and H. D. Cochran, J. Chem. Phys. **105**, 1214 (1996).
[10]R. Khare, J. de Pablo, and A. Yethiraj, J. Chem. Phys. **107**, 6956 (1997).
[11]A. Jabbarzadeh, J. D. Atkinson, and R. I. Tanner, J. Non-Newtonian Fluid Mech. **77**, 53 (1998).
[12]J. D. Moore, S. T. Cui, H. D. Cochran, and P. T. Cummings, J. Chem. Phys. **113**, 8833 (2000).
[13]S. Bair, C. McCabe, and P. T. Cummings, Phys. Rev. Lett. **88**, 058302 (2002).
[14]J. T. Bosko, B. D. Todd, and R. J. Sadus, J. Chem. Phys. **121**, 1091 (2004).
[15]C. Baig, B. J. Edwards, D. J. Keffer, H. D. Cochran, and V. A. Harmandaris, J. Chem. Phys. **122**, 184906 (2005).
[16]H.-C. Tseng, J.-S. Wu, and R.-Y. Chang, J. Chem. Phys. **129**, 014502 (2008).
[17]H.-C. Tseng, J.-S. Wu, and R.-Y. Chang, J. Chem. Phys. **130**, 084904 (2009).
[18]H.-C. Tseng, J.-S. Wu, and R.-Y. Chang, J. Chem. Phys. **130**, 164515 (2009).
[19]O. Borodin, G. D. Smith, and H. Kim, J. Phys. Chem. B **113**, 4771 (2009).
[20]A. Martini and A. Vadakkepatt, Tribol. Lett. **38**, 33 (2010).
[21]J. Petravic and J. Delhommelle, J. Chem. Phys. **122**, 234509 (2005).
[22]D. R. Wheeler and R. L. Rowley, Mol. Phys. **94**, 555 (1998).
[23]S. Balasubramanian, C. J. Mundy, and M. L. Klein, J. Chem. Phys. **105**, 11190 (1996).
[24]M. Kröger and S. Hess, Phys. Rev. Lett. **85**, 1128 (2000).
[25]J. D. Moore, S. T. Cui, H. D. Cochran, and P. T. Cummings, J. Non-Newtonian Fluid Mech. **93**, 83 (2000).
[26]P. J. Daivis, M. L. Matin, and B. D. Todd, J. Non-Newtonian Fluid Mech. **111**, 1 (2003).
[27]A. Jabbarzadeh, J. D. Atkinson, and R. I. Tanner, Macromolecules **36**, 5020 (2003).
[28]J. T. Bosko, B. D. Todd, and R. J. Sadus, J. Chem. Phys. **121**, 12050 (2004).
[29]K. Foteinopoulou, N. C. Karayiannis, and V. G. Mavrantzas, Macromolecules **39**, 4207 (2006).
[30]J. M. Kim, B. J. Edwards, and D. J. Keffer, J. Mol. Graphics. Modell. **26**, 1046 (2008).
[31]T. A. Hunt and B. D. Todd, Mol. Simul. **35**, 1153 (2009).
[32]J. T. Bosko, B. D. Todd, and R. J. Sadus, J. Chem. Phys. **123**, 034905 (2005).
[33]T. Kairn, P. J. Daivis, I. Ivanov, and S. N. Bhattacharya, J. Chem. Phys. **123**, 194905 (2005).
[34]J. Delhommelle and J. Petravic, J. Chem. Phys. **118**, 2783 (2003).
[35]N. Galamba, C. A. Nieto de Castro, and J. F. Ely, J. Chem. Phys. **122**, 224501 (2005).
[36]R. B. Bird, R. C. Armstrong, and O. Hassager, *Fluid Mechanics*, 2nd ed. *Dynamics of Polymeric Liquids*, Vol. **1** (Wiley-Interscience, New York, 1987).
[37]J. D. Moore, S. T. Cui, H. D. Cochran, and P. T. Cummings, J. Non-Newtonian Fluid Mech. **93**, 101 (2000).
[38]J. Delhommelle and D. J. Evans, J. Chem. Phys. **115**, 43 (2001).
[39]P. J. Daivis, D. J. Evans, and G. P. Morriss, J. Chem. Phys. **97**, 616 (1992).
[40]Z. Xu, J. J. de Pablo, and S. Kim, J. Chem. Phys. **102**, 5836 (1995).
[41]J.-C. Wang and K. A. Fichthorn, J. Chem. Phys. **109**, 10138 (1998).
[42]L. I. Kioupis and E. J. Maginn, J. Phys. Chem. B **104**, 7774 (2000).
[43]M. P. Allen and D. J. Tildesley, *Computer Simulation of Liquid* (Clarendon, Oxford, 1989).
[44]J.-P. Ryckaert and A. Bellemans, Chem. Phys. Lett. **30**, 123 (1975).
[45]S. Chynoweth and Y. Michopoulos, Mol. Phys. **81**, 133 (1994).
[46]D. N. J. White and M. J. Bovill, J. Chem. Soc., Perkin Trans. **2**, 1610 (1977).
[47]D. Macgowan and D. M. Heyes, Mol. Simul. **1**, 277 (1988).
[48]J. H. Ferziger and M. Peric, *Computational Methods for Fluid Dynamics*, 3rd ed. (Springer Science, Berlin, 2002).
[49]Y. Tsuchiya, H. Hasegawa, and T. Iwatsubo, J. Chem. Phys. **114**, 2484 (2001).
[50]P. J. Flory, *Statistical Mechanics of Chain Molecules* (Hanser Publishers, Munich, 1989).
[51]K. P. Travis and D. J. Evans, Mol. Simul. **17**, 157 (1996).
[52]S. Fujiwara and T. Sato, J. Chem. Phys. **107**, 613 (1997).
[53]R. G. Larson, *The Structure and Rheology of Complex Fluids* (Oxford University Press, New York, 1999).
[54]P. V. K. Pant and R. H. Boyd, Macromolecules **25**, 494 (1992).
[55]J. M. Haile, *Molecular Dynamics Simulation*, 2nd ed. (Wiley-Interscience, New York, 1997).
[56]D. A. McQuarrie, *Statistical Mechanics* (University Science Books, Sausalito, 2000).
[57]G. Marcelli, B. D. Todd, and R. J. Sadus, Phys. Rev. E **63**, 021204 (2001).
[58]K. Rah and B. C. Eu, Physica A **292**, 102 (2001).
[59]H. A. Barnes, J. F. Hutton, and K. Walters, *An Introduction to Rheology* (Elsevier, New York, 1989).
[60]G. H. Goo, G. Sung, S. H. Lee, and T. Chang, Bull. Korean Chem. Soc. **23**, 1595 (2002).
[61]P. Padilla and S. Toxvaerd, J. Chem. Phys. **97**, 7687 (1992).
[62]D. E. Smith, H. P. Babcock, and S. Chu, Science **283**, 1724 (1999).

[63]T. C. Le, B. D. Todd, P. J. Daivis, and A. Uhlherr, J. Chem. Phys. **130**, 074901 (2009).
[64]J. M. Kim, D. J. Keffer, M. Kröger, and B. J. Edwards, J. Non-Newtonian Fluid Mech. **152** 168 (2008).
[65]D. A. Hajduk, P. Urayama, S. M. Gruner, S. Erramilli, R. A. Register, K. Brister, and L. J. Fetters, Macromolecules **28**, 7148 (1995).
[66]A. Ciferri, C. A. J. Hoeve, and P. J. Flory, J. Am. Chem. Soc. **83**, 1015 (1961).
[67]X. Wang and C. Wu, Macromolecules **32**, 4299 (1999).
[68]I. Teraoka, *Polymer Solutions* (Wiley-Interscience, New York, 2002).
[69]P. E. Boukany, P. Tapadia, and S.-Q. Wang, J. Rheol. **50**, 641 (2006).
[70]S. G. Advani and C. L. Tucker, J. Rheol. **34**, 367 (1990).
[71]J. S. Cintra, Jr. and C. L. Tucker, J. Rheol. **39**, 1095 (1995).
[72]J. Wang, J. F. O'Gara, and C. L. Tucker, J. Rheol. **52**, 1179 (2008).